A Near-Infrared Imaging Survey of Coalsack Globule 2

Germán Racca[1], Mercedes Gómez[2]

Observatorio Astronómico de Córdoba, Laprida 854, 5000 Córdoba, Argentina

german@oac.uncor.edu, mercedes@oac.uncor.edu

and

Scott J. Kenyon[2]

Smithsonian Astrophysical Observatory, 60 Garden Street, Cambridge MA 02138

skenyon@cfa.harvard.edu

ABSTRACT

We describe a near-infrared imaging survey of Globule 2 in the Coalsack. This Bok globule is the highest density region of this southern hemisphere molecular cloud and is the most likely location for young stars in this complex. The survey is complete for $K < 14.0$, $H < 14.5$, and $J < 15.5$, several magnitudes more sensitive than previous observations of this globule. From the large number of background stars, we derive an accurate near-infrared extinction law for the cloud. Our result, $E_{J-H}/E_{H-K} = 2.08 \pm 0.03$, is significantly steeper than results for other southern clouds. We use the $J - H/H - K$ color-color diagram to identify two potential young stars with $K < 14.0$ in the region. We apply H-band star counts to derive the density profile of the Coalsack Globule 2 and use a polytropic model to describe the internal structure of this small cloud. For a gas temperature T $\sim$ 15 K, this globule is moderately unstable.

Subject headings: ISM: individual (Coalsack) — ISM: dust, extinction — ISM: globules — star: formation — star: pre-main sequence

1. Introduction

The Coalsack is a conspicuous, nearby (**?**, d $\sim$ 180 pc;)]fra89 dark cloud located close to the Galactic plane in the southern Milky Way (l $\sim 303^o$, b $\sim 0^o$). Nyman et al. (1989) estimated a

[1]Also at the Facultad de Matemática, Astronomía y Física, Universidad Nacional de Córdoba, Argentina.

[2]Visiting Astronomer, Cerro Tololo Inter-American Observatory. CTIO is operated by AURA, Inc. under contract to the National Science Foundation.

total mass of $\sim$ 3550 $M_\odot$ from ^{12}CO data covering an area of $\sim$ 15 deg^2 in the direction of this complex. Star counts toward the same area indicate an average optical extinction of $A_V \sim 5$ mag (Gregorio-Hetem et al. 1988; Cambrésy 1999). However, the extinction is $A_V \sim 20$ mag or larger in several small dark globules (Tapia 1973; Hartley et al. 1986; Bourke et al. 1995a). This structure is similar to other well-known clouds such as Taurus, Chamaeleon I, and Lupus that are actively forming stars (Cernicharo & Bachiller 1984; Boulanger et al. 1998; Arce & Goodman 1999; Cambrésy 1999). Despite this similarity, previous searches of the Coalsack have failed to detect signs of recent star-formation (Weaver 1974; Schwartz 1977; Reipurth 1981; Nyman et al. 1989).

Recently Kato et al. (1999) have observed the Coalsack in the ^{13}CO and C^{18}O J=1–0 lines. The ^{13}CO data show a massive cloudlet ($\sim$ 200 $M_\odot$) located at the western edge of the complex, coinciding with the region of the largest optical extinction (**?**, see)]cam99. In addition, these authors identified five C^{18}O cores (**?**, see also)]vil94, corresponding to the positions of well-known optically dark globules (Tapia 1973; Hartley et al. 1986; Bourke et al. 1995a). These cores have high column densities, typical of star-forming cores, and masses between 4–10 $M_\odot$. However, there are no *IRAS* sources, and thus no evidence of recent star-formation, in these cores (Kato et al. 1999).

Tapia's Globule 2 ($\alpha = 12^h\ 31.5^m$, $\delta = -63^o\ 44.5'$; 2000.0) is the densest (n(H$_2$) $\sim 4 \times 10^3$ cm^{-3}) and most massive ($\sim$ 10 $M_\odot$) of the Kato et al. cores (**?**, see also)]bou95b. It is an obvious, roughly circular patch (**?**, $\sim 6'$ radius;)]bou95a of extinction on shallow optical and near-infrared (near-IR) surveys. Jones et al. (1980) observed an area of $\sim$ 850 arcmin^2 to $K = 9.5$; Jones et al. (1984) scanned an area of $2' \times 2'$, 70% complete to $K = 13.7$, with the central $1' \times 1'$ region 70% complete to $K = 14.7$. Neither of these surveys detected candidate near-IR excess stars. At $K = 9.5$, Jones et al. (1980, 1984) could detect $\sim$ 1 $M_\odot$ main sequence stars at the distance of the Coalsack. In the central $1' \times 1'$ region, 70% complete to $K = 14.7$, this detection limit is $\sim$ 0.4 $M_\odot$, assuming $A_K \sim 2$ (**?**, see)]hemc93,del00.

The Coalsack Globule 2 has also been observed by the *Midcourse Space Experiment* (**?**, MSX;)]pri01. Fits format images and a source catalog in four mid-infrared bands, A(8.28 μm), C(12.13 μm), D(14.65 μm), and E(21.34 μm), are available through the NASA/IPAC IR Science Archive (IRSA)[3]. Nine mid-infrared sources lie within $\sim 11'$ from the optical center of the globule. One of these is located $\sim 2.8'$ SW from the center of the most massive Kato et al. C^{18}O cores. This different is comparable to the $2'$ resolution of the molecular line maps.

Here, we describe a near-IR imaging survey of $\sim 15' \times 15'$ centered on Globule 2. The observations are uniformly complete to $K = 14.0$, $H = 14.5$, and $J = 15.5$. If $A_K \sim$ 0–2 mag, these data are sensitive to $\sim$ 0.2–0.5 $M_\odot$ main sequence stars (**?**, see)]hemc93,del00. We detect $\sim$ 6500 sources to the detection limits of $K = 16.5$, $H = 17.0$, and $J = 18.0$. We restrict our analysis to $K = 14.0$ ($\sim$ 2500 sources) where the photometric errors are relatively small (< 0.08 mag).

[3]http://irsa.ipac.caltech.edu.

In §2 we describe the observations and data reduction. In §3 we derive a reliable extinction curve for background stars in the Globule 2 region and use this result in §4 to search for potential young stellar objects in our survey region based on their locations in the $J - H/H - K$ diagram. We identify only two objects with $K < 14.0$ and near-IR excesses characteristic of young stellar objects. In §5 we use H-band stars counts to derive the density profile of this small cloud and compare it with the predictions of polytropic models. Assuming T $\sim$ 15 K, Globule 2 is moderately unstable. We conclude with a brief summary in §6.

2. Observations and Data Analysis

We obtained JHK imaging data for Globule 2 in the Coalsack and four relatively unreddened control fields on 13–16 February 1995, and 8–11 March 1996, with CIRIM (the Cerro Tololo Infrared Imager) at the CTIO 1.5m telescope. The CIRIM uses a 256 $\times$ 256 HgCdTe NICMOS 3 array, which provides a field of $\sim 4.9' \times 4.9'$ with a plate scale of $1.16''$ per pixel. We covered an area of $\sim 15' \times 15'$ on the cloud on a regular grid, with $1'$ overlap between adjacent frames. We acquired two 6 $\times$ 5 sec exposures for each field, shifted by $20''$. We also observed four $5' \times 5'$ control fields, selected from a visual inspection of the ESO Red Sky Survey prints, close to Globule 2 region and relatively free from significant optical extinction. Table 1 lists positions of these off-cloud regions.

We process the data using standard techniques with the IRAF[4] software package. Gómez & Kenyon (2001) describes the data reduction procedure in detail. Briefly, we apply dark, flatfield, and sky corrections to all images, align dithered pairs using the IRAF subroutines GEOMAP and GEOTRAN, and then add the dithered pairs. We select the K images as the reference frames and transform the J and H images to the same pixel scale as the K images. We use DAOFIND to locate stars 4σ above the local background and add to the DAOFIND list all stellar objects missed by this routine and found by visual inspection of each image. We then derive photometry for each image using the APPHOT PHOT task, using a circular aperture with $5''$ radius. We detect $\sim$ 6500 sources at JHK in our survey region.

To calibrate our photometry, we observed on each night a set of 10-15 standards from Elias et al. (1982) and from the UKIRT faint JHK standard stars list (Hawarden et al. 2001). Gómez & Kenyon (2001) estimate photometric uncertainties of $\pm$ 0.03 mag in this calibration. These authors also list typical photometric uncertainties in each magnitude bin. These uncertainties reach 0.3 mag for $J \sim 17$, $H \sim 16$, and $K \sim 15$. The 5σ limiting magnitudes are $K = 14.5$, $H = 15.5$, and $J = 16.0$. The magnitudes are in the CIT (Elias et al. 1982) system (**?**, see)]goke01.

To check the completeness of the survey, we construct a list of detected sources. Figure 1 shows the magnitude histograms of background stars as functions of JHK. The number of stars per bin

[4]IRAF is distributed by the National Optical Astronomy Observatory, which is operated by the Association of Universities for Research in Astronomy, Inc. under contract to the National Science Foundation.

increases monotonically up to the completeness limit and then turns over. The corresponding limits in each filter are $J = 15.5$, $H = 14.5$, and $K = 14.0$.

To derive coordinates for our survey stars, we use WCSTools[5] (Mink 1997), a suite of programs to calculate a direct transformation between the coordinates of the image (x,y) and the sky coordinates (α,δ). We measure the transformation coefficients adopting matches between program stars and stars in the U.S. Naval Observatory SA1.O Catalogue (Monet et al. 1996). We estimate an average uncertainty in our positions of $1''$. This estimate relies on a direct comparison of our coordinates with coordinates from the Digitized Sky Survey[6] (DSS).

3. The Coalsack Globule 2 Near-Infrared Reddening Law

We use a general photometric technique to derive the near-IR reddening law in the Coalsack (Kenyon et al. 1998). The technique assumes that the stellar population behind the cloud is identical to the stellar population in off-fields several degrees away. Because the Coalsack contains so few pre-main sequence stars, this assumption is reasonable. Kenyon et al. (1998) derive the $J-H$ and $H-K$ color excesses for each on-cloud source relative to every off-cloud source and then compute the average and median color excesses for each on-cloud source. The probable error of the average color excess is the sum in quadrature of the errors of the on-cloud and off-cloud colors. For the median color excess, the probable error is the inter-quartile range.

Figure 2 shows average color excesses of Coalsack stars with K $\leq$ 14. We consider stars with $K < 14.0$, where the photometric errors are $\lesssim 0.1$ mag. We eliminate two potential young stars with near-IR excesses from this analysis (see §4 below). The color excesses are correlated, with a Spearman rank-order correlation coefficient of $r_s = 0.88$. The probability for no correlation between the two color excesses is formally zero according to the Spearman rank-order test. Straight line fits to color excess measurements yield $E_{J-H}/E_{H-K} = 2.07 \pm 0.05$. Median color excesses for each source yield the same slope and error.

To test the robustness of the near-IR extinction law, Kenyon et al. (1998) define the reddening probability function. The reddening probability $\rho(E_x, E_y)$ is the chance of measuring a pair of color excesses E_x and E_y, where x and y are color indices and $N = \int \rho(E_x, E_y)\, dE_x dE_y$ is the number of reddening measurements. The number, N, is also the number of on-field stars in the sample. The

[5]Available at ftp://cfa-ftp.harvard.edu/pub/gsc/WCSTools

[6]Based on photographic data obtained using The UK Schmidt Telescope. The UK Schmidt Telescope was operated by the Royal Observatory Edinburgh, with funding from the UK Science and Engineering Research Council, until 1988 June, and thereafter by the Anglo-Australian Observatory. Original plate material is copyright (c) the Royal Observatory Edinburgh and the Anglo-Australian Observatory. The plates were processed into the present compressed digital form with their permission. The Digitized Sky Survey was produced at the Space Telescope Science Institute under US Government grant NAG W-2166. Copyright (c) 1993, 1994, Association of Universities of Research in Astronomy, Inc. All right reserved.

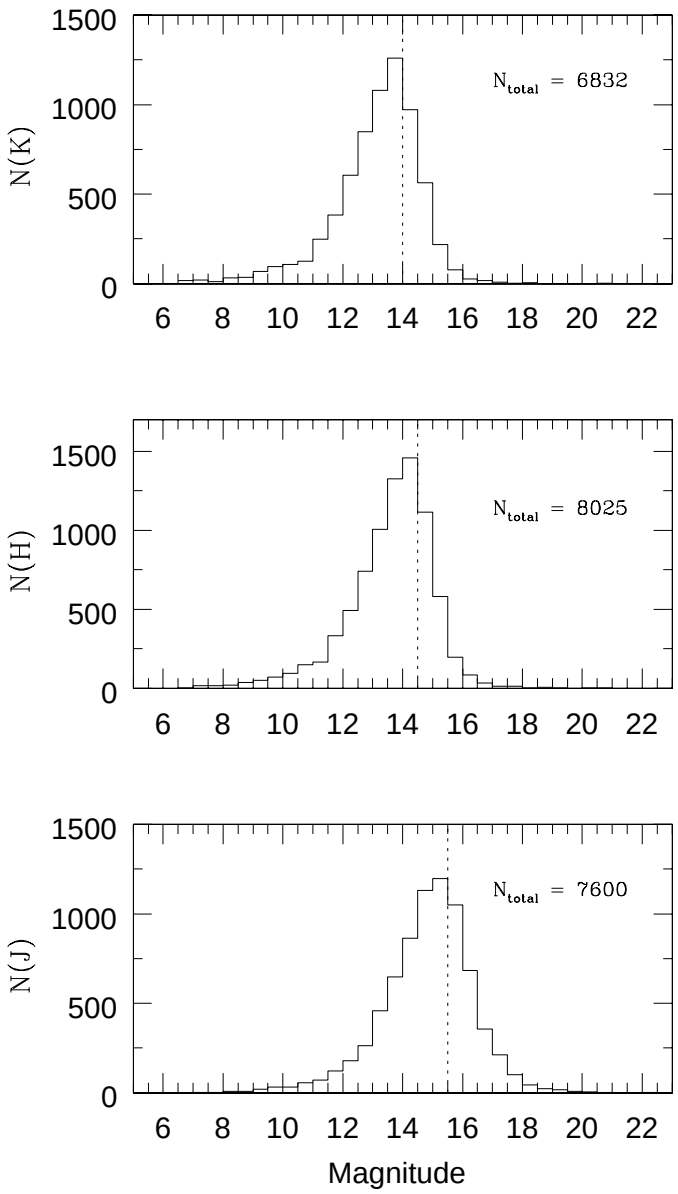

Fig. 1.— Histogram distribution of magnitudes for background stars in our survey region. The completeness limit in each band is indicated by the dashed vertical lines.

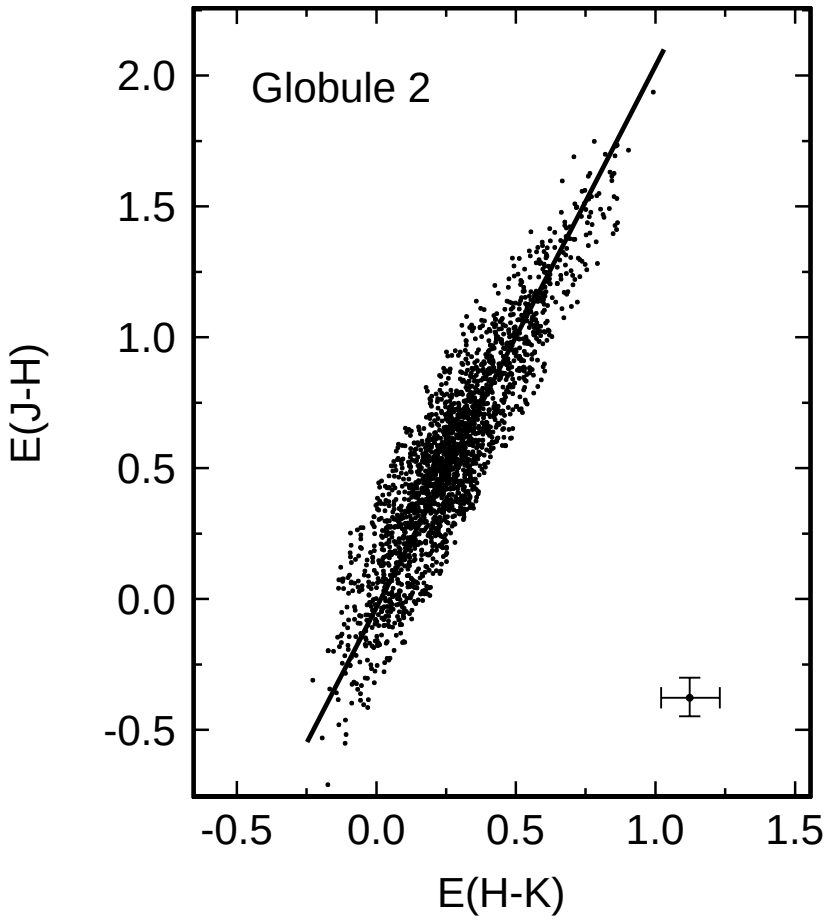

Fig. 2.— Average color-excess diagram for Globule 2 stars with $K < 14$. The sample includes 2271 stars used in the analysis.

density function, $\rho(E_x, E_y)$, depends on the distributions of colors in the on-field and the off-field and results from a convolution of the densities of off-field and on-field stars in the color-magnitude diagram (Kenyon et al. 1998). These color distributions use a kernel density estimator with smoothing parameter $h = 0.2$ to derive the density.

Figure 3 shows the probability functions for the Coalsack. The color-color diagram in the left panel shows the middle of the main sequence and the lower main sequence as peaks in the density. The middle panel indicates a clear peak in the sample of Coalsack stars at $H - K \approx 0.5$ and $J - H \approx 1.3$–1.5. The reddening probability function in the right panel consists of a collection of nested aligned ellipses. The major axes of these ellipses have a slope consistent with the slope of the reddening law in Figure 2, $E_{J-H}/E_{H-K} = 2.08 \pm 0.03$. Kenyon et al. (1998) describes the derivation of the slope of the major axis of each contour in Figure 3. The ellipses are symmetric about the reddening line, suggesting that the Coalsack contains few stars with near-IR excesses (see below).

The Coalsack near-IR extinction law is different from other near-IR extinction laws. In previous studies, we derive $E_{J-H}/E_{H-K} = 1.80 \pm 0.03$ for the Chamaeleon I dark cloud (Gómez & Kenyon 2001) and $E_{J-H}/E_{H-K} = 1.57 \pm 0.03$ for the ρ Ophiuchi dark cloud (Kenyon et al. 1998). The Cha I extinction law agrees with the standard extinction law of Bessell & Brett (1988), $E_{J-H}/E_{H-K} = 1.75$, transformed to the CIT system. The ρ Oph law is more similar to results from the He et al. (1995) survey of luminous southern stars, $E_{J-H}/E_{H-K} = 1.47 \pm 0.06$. The extinction laws for the three dark clouds differ by $\sim 10\sigma$, suggesting dramatic changes in grain composition or size between these clouds.

The ratio of total to selective extinction, R_V, may also to vary among dark clouds (**?**, see)and the references therein]ke98. Kim & Martin (1996) attribute this variation to different grain properties from cloud to cloud. Dense regions have larger R_V and fewer small grains than diffuse clouds. On average, grain sizes increase with cloud density. In addition, recent calculations show a clear dependence of the extinction law on the grain mixture and composition (**?**, see, for example,)]vai01.

Molecular line observations confirm the difference between Cha I and the Coalsack. Harjunpää & Mattila (1996) report a significant range in the ratio of the CO column density $N(CO)$ to the $J - K$ color excess E_{J-K} in several southern molecular clouds. The observed $N(CO)/E_{J-K}$ is a factor of two larger in Cha I than in the Coalsack. The R CrA star-forming region also has a large $N(CO)/E_{J-K}$. Harjunpää & Mattila (1996) suggest that $N(CO)/N(H_2)$ or $N(H_2)/E_{J-K}$ or both vary significantly between these clouds. Other clouds display similar variations. Kramer et al. (1999) note changes in $N(CO)/A_V$ within the dark cloud IC 5146, which they interpret as differences in the amount of CO depletion onto dust grains. From observations of $C^{17}O$, $C^{34}S$, and N_2H^+, Bergin et al. (2001) show that the pattern of gas depletion in IC 5146 is consistent with models of cloud chemistry.

Our observations of ρ Oph, Cha I, and the Coalsack indicate important differences in grain chemistry among dark clouds. Changes in the slope of the near-IR extinction law appear correlated

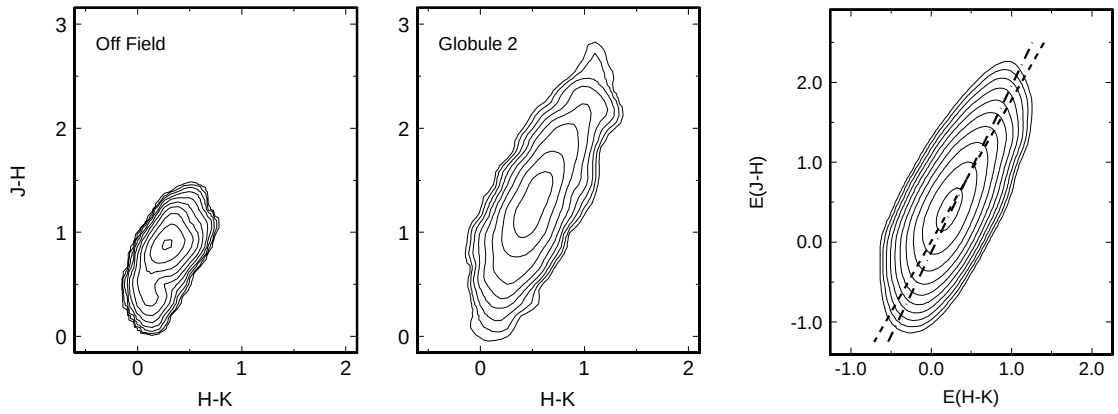

Fig. 3.— Density distributions for Globule 2 stars. The left and middle panels show the color density distributions for stars off the main Globule 2 field (off-field, left panel) and for stars projected on the globule (Globule 2, middle panel). The right panel plots the reddening probability distribution for the Globule 2 sources, assuming that these stars have the same color distribution as the off-field stars.

with the degree of star formation activity or the density of the cloud or both. ρ Oph is the most active star formation region of this group and it has the regions of largest extinction. The Coalsack is the most quiescent cloud and has the lowest extinction. Testing whether this correlation is real or a fluke of small number statistics requires high quality extinction measurements in more dark clouds.

4. Search for Candidate Pre-Main Sequence Stars

Figure 4 shows the $H-K/J-H$ diagram for our complete survey region. The solid line corresponds to the main sequence locus (Bessell & Brett 1988); the dashed lines, parallel to the reddening vector ($E_{J-H}/E_{H-K} = 2.08 \pm 0.03$) derived in §3, define the reddening band extending from the main sequence. We detect ~ 2500 stars in Globule 2 with $K < 14.0$.

We distinguish two groups of sources in Figure 4: i) stars that lie along or follow the reddening band direction, and ii) two sources with near-IR excess located to the right of the reddening band. The first group contains almost all of our detections. These objects are reddened main sequence or giant stars (see §3) and lie behind the cloud [7]. The color excesses of the second sample cannot be attributed to reddening by normal dust in the cloud. Circumstellar material (disks + infalling envelopes) surrounding the young central stars can produce these color excesses at near-IR wavelengths (Lada & Adams 1992; Kenyon & Hartmann 1995). Two stars in our sample have near-IR color excesses similar to previously known young stars Table 2 lists coordinates and magnitudes for these stars. They are located within $\sim$ 5–6′ of the position of the $C^{18}O$ core detected by Kato et al. (1999). In a similar manner, the nearest mid-infrared MSX sources to these candidates lie at distances of $\sim 5'$ and $3.5'$, respectively.

We find three objects in common between our near-infrared survey and the nine sources from the MSX catalog that lie within radius of $\sim 11'$ from the optical position of the Globule 2. The other 6 mid-infrared sources are located close but outside of our $15' \times 15'$ observed area.

Although the Coalsack lies in the general direction of the Sagittarius-Carina arm of the Milky Way, Nyman et al. (1989) note that there is no background cloud at the position of Globule 2. Confusion with background sources is not significant; the selected candidates probably belong to the Coalsack region lying in the vicinity of this globule. The near-IR excesses of these sources suggests the pre-main sequence nature of these stars. Optical spectroscopy is required to test this suggestion.

[7] Any weak emission T Tauri stars that belong to the cloud and that, as a class of young stellar objects, have no significant near-IR excess are included in this group.

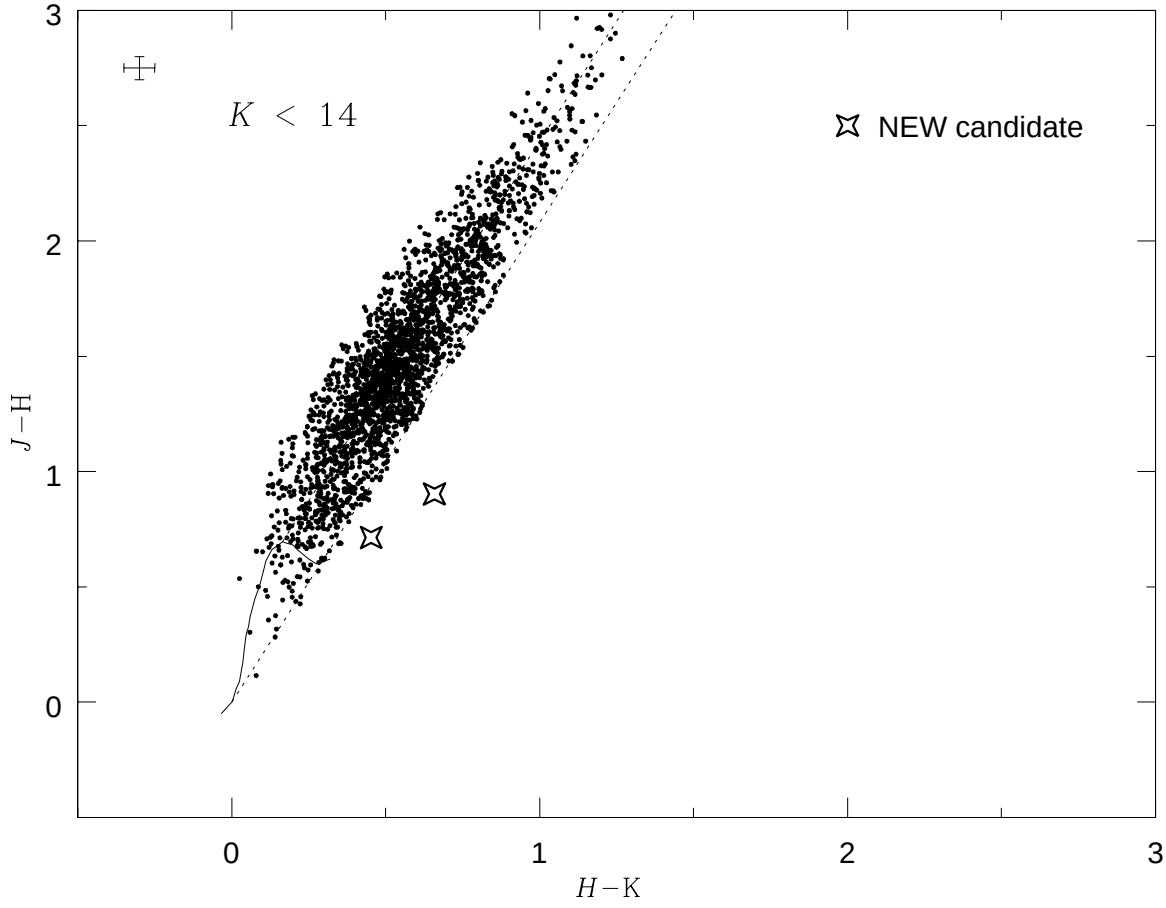

Fig. 4.— Color-color diagram for near-IR sources with $K < 14.0$ in our survey region. The solid line indicates the main sequence locus (Bessell & Brett 1988) and the two parallel lines define the reddening band, extending from the main sequence. To define this band we use the reddening vector, $E_{J-H}/E_{H-K} = 2.08 \pm 0.03$, derived in section 3. Typical photometric errors for $K \sim 14.0$ are displayed in the upper left corner. The big stars show the positions of two near-infrared candidate young stellar objects.

5. The Coalsack Globule 2 Density Profie

5.1. The Extinction Map

To map the distribution of extinction in Globule 2, we divide the observed region (a $15' \times 15'$ area) into a fixed grid of $1' \times 1'$ overlapping squares, separated by the $30''$ Nyquist spatial sampling interval. We follow the same procedure for our off-cloud regions (see Table 1). H-band star counts in these two areas then yield an extinction map. This standard method compares the stellar density in each position of the cloud with the density in a nearby control area assumed free of significant obscuration. The number of stars per unit area brighter than m_λ in the control field, N_{off}, is

$$\mathrm{Log\ N_{off}} = \mathrm{a} + \mathrm{b\ m}_\lambda\ . \tag{1}$$

On the cloud, the slope of equation (1) remains the same but the number of stars per unit area, N_{on}, decreases as the extinction Am_λ increases. The extinction is then

$$\mathrm{Am}_\lambda = \frac{1}{\mathrm{b}}\ \mathrm{Log}\ \frac{\mathrm{N_{off}}}{\mathrm{N_{on}}}, \tag{2}$$

where b is the slope of the cumulative luminosity function. We use the H-band luminosity function for off cloud regions to measure $\mathrm{b} = 0.32 \pm 0.01$. We convert the H-band extinction, A_H, to optical extinction, A_V, using the Rieke & Lebofsky (1985) reddening law ($A_V = 5.7\ A_H$) and convolve the individual stellar measurements with a two dimensional Gaussian filter with a FWHM of $60''$, the size of our grid cells. Large cells yield poor resolution; smaller cells have too few stars for a meaningful measurement. Figure 5 shows our extinction map. The smoothed stellar positions display roundish shapes. The outermost contour corresponds to $A_V = 5$. Subsequent contours increase in steps of 3 mag, reaching $A_V = 23$ mag in the innermost area. As noticed by Jones et al. (1984), Globule 2 is embedded in the Coalsack; the 5 mag level is probably the average level of dust absorption in the surrounding cloud region.

We determine mean radii for each optical obscuration level, normalize this 'average' density with respect to the 23 mag peak level, and plot the results in Figure 6 as dot symbols. The projected radial dust column density distribution is shallow, suggesting a configuration near equilibrium. Density profiles of unstable clouds show a clear enhancement toward the center, indicating the collapse of material (**?**, see)]har01.

5.2. The Polytropic and the Bonnor-Ebert Models

To model the internal structure of Globule 2, we consider the Lane-Emden equation for a self-gravitating isothermal gas sphere in hydrostatic equilibrium:

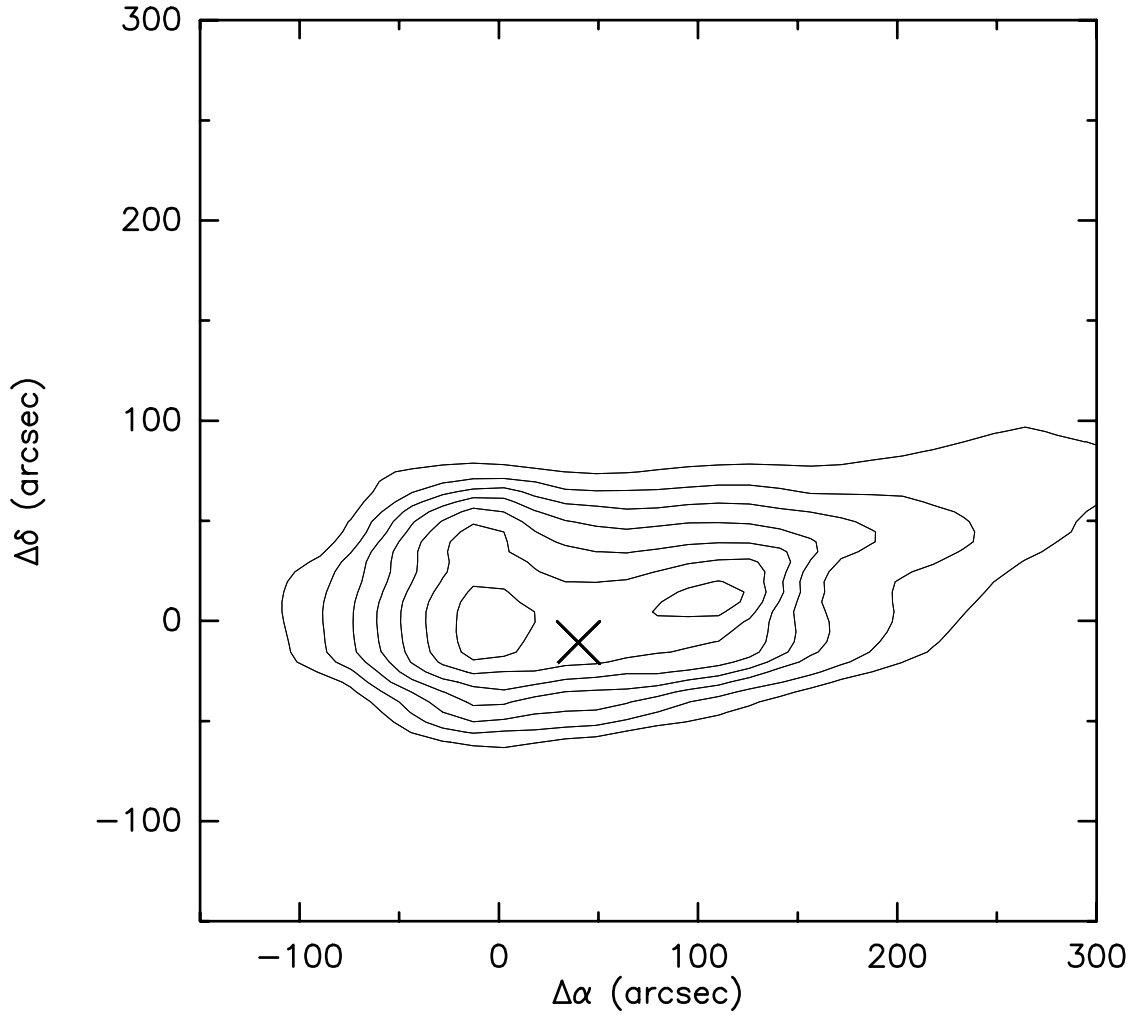

Fig. 5.— Extinction map for the Globule 2. The lowest contour corresponds to $A_V = 5$ mag. Subsequent contours increase in step of 3 mag. The coordinates of the center of the region are: $\alpha(2000.0) = 12^h\ 31^m\ 24^{sec}$, $\delta(2000.0) = -\ 63^o\ 45'\ 11''$. The big cross indicates the position of the Kato et al. (1999) $C^{18}O$ core.

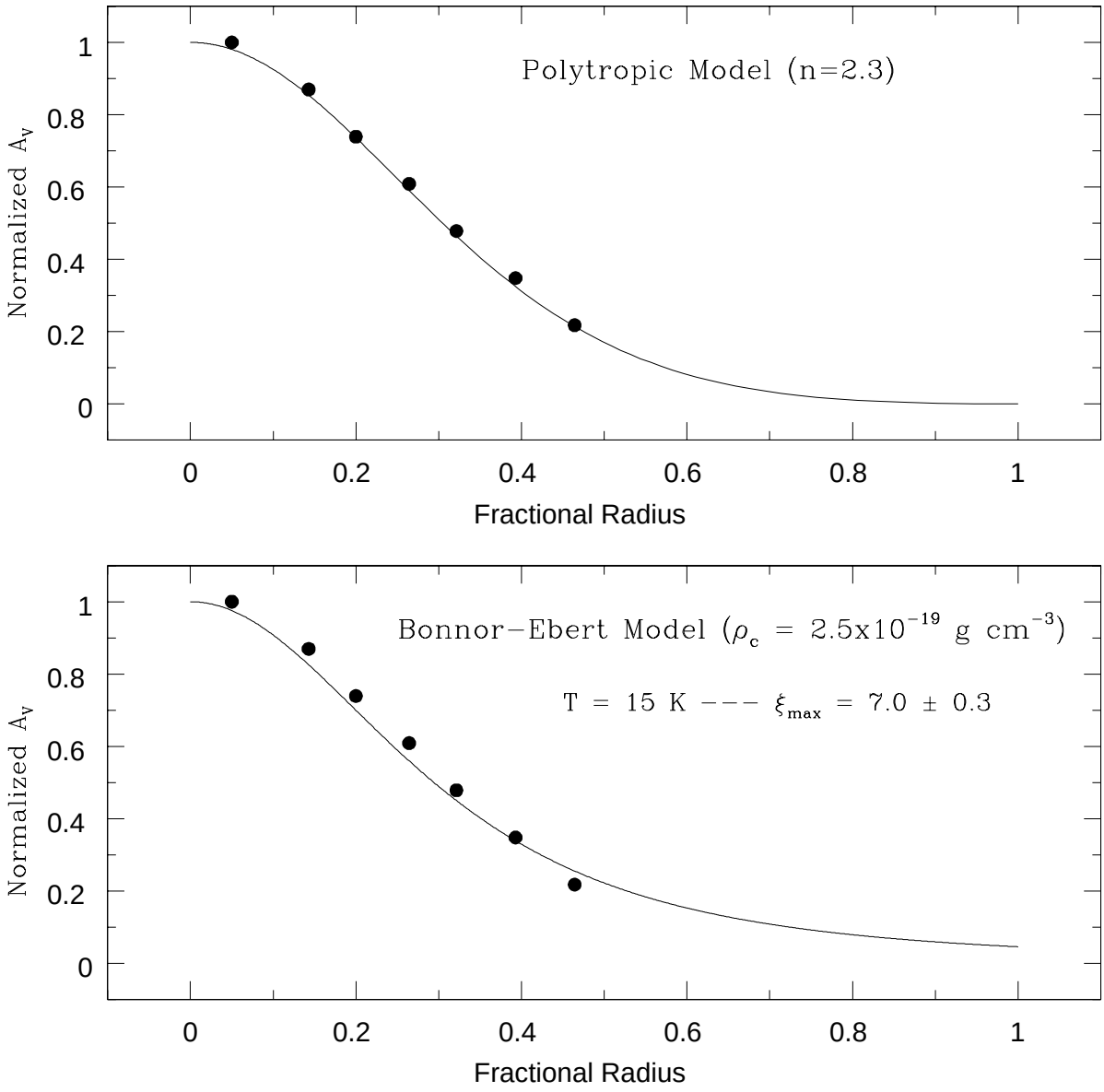

Fig. 6.— Normalized density profile for the Globule 2. The optical extinction A_V is referred to the central peak value (23 mag). The radial distance is the fractional radius with respect to R = 140″ ($\sim$ 0.1 pc), corresponding to A_V = 5 mag. The dot symbols represent our observational data and the continuous lines the model fits. The upper panel corresponds to a polytrope with n = 2.3. The lower panel indicates the Bonnor-Ebert model for a central density $\rho_c = 2.5 \times 10^{-19}$ g/cm^3, assuming T = 15 K for this globule.

$$\frac{1}{\xi^2}\frac{\mathrm{d}}{\mathrm{d}\xi}(\xi^2\frac{\mathrm{d}\theta}{\mathrm{d}\xi}) = -\theta^{\mathrm{n}}, \tag{3}$$

where $\xi = \mathrm{r}/\alpha$ and $\theta = \mathrm{T}/\mathrm{T}_c$ are the Emden variables, with α an unspecified factor having dimensions of length and T_c the central temperature (**?**, see, for example,)]nov73. The parameter 'n' is the polytropic index relating the gas pressure to the density, $P_{gas} = K_n\rho^n$. We consider two approaches to solve equation (3): a) a numerical integration for specific values of 'n' and b) the introduction of a variant of this pressure-confined, self-gravitating isothermal sphere equation.

Kenyon & Starrfield (1979) adopted the first approach and numerically solved equation (3) for different values of the polytropic index n, satisfying the following boundary conditions: $\theta = 1$ and $\mathrm{d}\theta/\mathrm{d}\xi = 0$ at $\xi = 0$. The upper panel of Figure 6 shows the normalized density profile superposed on a polytropic model with index n = 2.3. We adopt an 'average' external radius of 140″, 0.1 pc at the distance of the this cloud. This radius corresponds to $\mathrm{A}_V = 5$ mag, which we assume represents the average optical extinction in the surrounding Coalsack region. For n = 2.3., Kenyon & Starrfield (1979)'s calculations predict a central density $\rho_c = 3 \times 10^{-19}$ g/cm^3 and a temperature T = 20 K to support the cloud against collapse. Although we have no direct temperature measurement of Globule 2, the average temperature for other small globules is T = 10–15 K (Bourke et al. 1995b). The factor of 1.2–2.0 difference between the 'observed' and hydrostatic equilibrium temperature suggests that Globule 2 is marginally unstable and on the verge of collapse.

In our second approach, we consider a variant of equation (3), known as the Bonnor-Ebert model (Bonnor 1956; Ebert 1955) or the modified Lane-Emden equation:

$$\frac{1}{\xi^2}\frac{\mathrm{d}}{\mathrm{d}\xi}(\xi^2\frac{\mathrm{d}\phi}{\mathrm{d}\xi}) = \mathrm{e}^{-\phi}, \tag{4}$$

where $\rho = \rho_c e^{-\phi(\xi)}$. Here, $\xi = (r/a)\sqrt{4\pi G\rho_c}$ is a dimensionless radial parameter and a is the isothermal sound speed ($a = \sqrt{kT/\mu m_{\mathrm{H}}}$; μ is the mean molecular weight and m_{H} is the mass of the H atom). Introducing standard boundary conditions ($\phi(0) = 0$ and $\mathrm{d}\phi(0)/\mathrm{d}\xi = 0$), we solve equation (4) numerically. Assuming an external radius R (140″ or 0.1 pc), solutions of equation (4) can be parametrized by ρ_c. The lower panel of Figure 6 shows our best fit for $\rho_c = 2.5 \times 10^{-19}$ g/cm^3 superposed on the Globule 2 density profile. This solution assumes T= 15 K as a typical temperature for Bok globules (**?**, see)]bou95b and $\mu = 2$.

Bonnor (1956) demonstrated that the value of ξ at the external radius (R), $\xi_{\mathrm{max}} = \mathrm{R}/a\ \sqrt{4\pi G\rho_c}$ provides a stability measure. Systems with $\xi_{\mathrm{max}} > 6.5$ are unstable to gravitational collapse. For Globule 2, $\xi_{\mathrm{max}} = 7.0 \pm 0.3$ exceeds the critical value and is moderately unstable.

The mass of the globule and the pressure at its outer boundary are functions of ξ:

$$\mathrm{M}(\xi) = 4\pi\beta^3\rho_{\mathrm{c}}(\xi^2\frac{\mathrm{d}\phi}{\mathrm{d}\xi}) \tag{5}$$

$$P(\xi) = a^2 \rho_c \, e^{-\phi(\xi)}, \tag{6}$$

where $\beta = a/\sqrt{4\pi G \rho_c}$. Evaluating these expressions at r = R (or $\xi = \xi_{max}$), we derive M = 4.5 $M_\odot$ and $P_{ext} = 9 \times 10^{-12}$ dyn/cm^2. Kato et al. (1999) estimate 10 $M_\odot$; our external pressure is roughly about 6.5 times the value for the interstellar medium (**?**, see)]elm91.

Both the polytropic and the Bonnor-Ebert models predict a moderately unstable configuration for Globule 2. The 'typical' T $\sim$ 10-15 K is a factor of 2 lower than the minimum value required for hydrostatic equilibrium. Magnetic fields may help to prevent the collapse. Jones et al. (1984) found evidence of a mildly compressed magnetic field from *H*-band polarization measurements of background stars in the Globule 2 region. The very modest intensities of magnetic fields associated with dark clouds (**?**, B $\sim$ 16 μG;)]cru93 suggest, however, that magnetic fields can not prevent the collapse indefinitely and alter the global process significantly.

Alves et al. (2001) used the Lane-Emden equation to fit the density profile of Barnard 68 (Bok 1977), an isolated nearby (d = 125 pc) southern hemisphere Bok globule. They derived $\xi_{max} = 6.9 \pm 0.2$, slightly larger than the critical value. B68 has a radius of 0.06 pc, M = 2.1$M_\odot$, T = 16 K, and an external pressure of 2.5×10^{-11} dyn/cm^2. This starless globule shows no evidence of star-formation and thus may be about to collapse to form stars.

Harvey et al. (2001) analyzed the dense globule in B335 (**?**, d $\sim$ 250 pc;)]tom79. The shape of the B335 density profile is steeper than either Globule 2 or B68. Harvey et al. (2001) show that collapse models and an unstable Bonnor-Ebert sphere (with $\xi_{max} = 12.5 \pm 2.6$) match the observed density profile. Molecular line profiles provide additional evidence that this globule is collapsing (Zhou et al. 1993; Choi et al. 1995). B335 is associated with a deeply embedded young stellar object (Keene et al. 1983) that drives a bipolar outflow (Cabrit et al. 1988; Hirano et al. 1988, 1992). Thus this core is in a more advanced evolutionary stage than B68.

The Coalsack Globule 2 may represent an intermediate phase between B68 (a pre-collapse globule) and B335 (an already collapsing core) according to the polytropic models and Bonnor's critical parameter, ξ_{max}.

6. Summary

Our near-IR survey of Globule 2, the highest density and more massive core in the Coalsack complex, leads to three primary conclusions.

The slope of the near-IR extinction law in the cloud, $E_{J-H}/E_{H-K} = 2.08 \pm 0.03$, is much steeper than in ρ Ophiuchi or Chamaeleon I. If real, the trend of increasing slope with decreasing star-formation activity in these three clouds suggests changes in grain chemistry with extinction or star formation activity.

Based on near-IR excess emission, we detect two pre-main sequence candidates with $K < 14$ in the vicinity Globule 2. If confirmed as pre-main sequence stars with optical or near-IR spectroscopy, these are the first pre-main sequence stars discovered in the region. The globule contains no known IRAS sources (Nyman et al. 1989; Bourke et al. 1995a) or other pre-main sequence candidates. Our candidates are too faint for detection with IRAS. The low success rate in finding pre-main sequence stars in the Globule 2 region illustrates the low activity of the Coalsack as stellar nursery, in agreement with previous investigations (Weaver 1974; Schwartz 1977; Reipurth 1981; Nyman et al. 1989).

We use H-band star counts to derive the density profile of this Bok globule. For a 'typical' gas temperature T $\sim$ 15 K, model fits suggest this small cloud is moderately unstable, with a Bonnor critical parameter $\xi_{\rm max} = 7.0 \pm 0.3$. The mass derived from these models, $M = 4.5 M_{\odot}$, agrees with estimates derived from the CO column density.

We are grateful to the CTIO staff, specially to M. Fernández, M. Hernández, and P. Ugarte for assistance during the observing runs. We also thank R. Elston and R. Probst for their help with CIRIM and D. Mink for assistance with the WCSTools software. An anonymous referee carefully read the original manuscript and provided useful suggestions.

REFERENCES

Alves, J. F., Lada, C. J., & Lada, E. A. 2001, Nature, 409, 159

Arce, H., & Goodman, A. A. 1999, ApJ, 517, 264

Bergin, E. A., Ciardi, D. R., Lada, C. J., Alves, J., & Lada, E. A. 2001, ApJ, 557, 209

Bessell, M. S., & Brett, J. M. 1988, PASP, 100, 1134

Bok, B. 1977, PASP, 89, 597

Bonnor, W. 1956, MNRAS, 116, 351

Boulanger, F., Bronfman, L., Dame, T. M., & Thaddeus, P. 1998, A&A, 332, 273

Bourke, T. L., Hyland, A. R., & Robinson, G. 1995a, MNRAS, 276, 1052

Bourke, T. L., Hyland, A. R., Robinson, G., James, S. D., & Wright, D. M. 1995b, MNRAS, 276, 1052

Cabrit, S., Goldsmith, P. F., & Snell, R. L. 1988, ApJ, 334, 196

Cambrésy, L. 1999, A&A, 345, 965

Cernicharo, J., & Bachiller, R. 1984, A&AS, 58, 327

Choi, M., Evans II, N. J., Gregerson, E. M., & Wang, Y. 1995, ApJ, 448, 742

Crutcher, R. M., Troland, T. H., Goodman, A. A., Heile, C., Kazes, I., & Myers, P. C. 1993, ApJ, 407, 175

Delfosse, X., Forveille, T., Ségransan, D., Beuzit, J.-L., Udry, S., Perrier, C., & Mayor, M. 2000, A&A, 364, 217

Ebert, R. 1955, Z. Astrophysik, 37, 217

Elias, J., Fogel, J. A., Matthews, K., & Neugebauer, G. 1982, AJ, 87, 1029

Elmegreen, B. G. 1991, In: Lada, C. J. & Kylafis, N. D. (eds.) The Physics of Star Formation and Early Stellar Evolution, 35 (Dordrecht:Kluwer)

Franco, G. A. P. 1989, A&A, 215, 119

Gómez, M., & Kenyon, S. J. 2001, AJ, 121, 974

Gregorio Hetem, J. C., Sanzovo, G. C., & Lépine, J. R. D. 1988, A&AS, 76, 347

Harjunpää, P., & Mattila, K. 1996, A&A, 305, 920

Hartley, M., Manchester, R. N., Smith, R. M., Tritton, S. B., & Goss, W. M. 1986, A&AS, 63, 27

Harvey, D. W. A., Wilner, D. J., Lada, C. J., Myers, P. C., Alves, J. F., & Chen, H. 2001, ApJS, 563, 903

Hawarden, T. G., Leggett, S. K., Letawsky, M. B., Ballantyne, D. R., & Casali, M. M. 2001, MNRAS, 325, 563

Henry, T., & McCarthy, Jr. D. W. 1993, AJ, 106, 773

He, L., Whittet, D. C. B., Kilkenny, D., & Spencer Jones, J. H. 1995, ApJS, 101, 335

Hirano, N., Kameya, O., Kasuga, T., & Umemoto, T. 1992, ApJL, 390, 85

Hirano, N., Kameya, O., Nakayama, M., & Takakubo, K. 1988, ApJL, 327, 69

Jones, T. J., Hyland, A. R., Robinson, G., Smith, R., & Thomas, J. 1980, ApJ, 242, 132

Jones, T. J., Hyland, A. R., & Bailey, J. 1984, ApJ, 282, 675

Kato, S., Mizuno, N., Asayama, S., Mizuno, A., & Ogawa, H. 1999, PASJ, 51, 883

Keene, J., Davidson, J. A., Harper, D. A., Hildebrand, R. H., Jaffe, D. T., Loewenstein, R. F., Low, F. J., & Pernic, R. 1983, ApJL, 274, 43

Kenyon, S. J., & Hartmann, L. 1995, ApJS, 101, 117

Kenyon, S. J., Lada, E. A., & Barsony, M. 1998, AJ, 115, 252

Kenyon, S. J., & Starrfield, S. 1979, PASP, 91, 271

Kim, S-H., & Martin, P. G. 1996, ApJ, 462, 296

Kramer, C., Alves, J., Lada, C. J., Lada, E. A., Sievers, A., Ungerechts, H., & Walmsley, C. M. 1999, A&A, 342, 257

Lada, C. J., & Adams, F. C. 1992, ApJ, 393, 278

Lawson, W. A., Feigelson, E. D., & Huenemoerder, D. P. 1996, MNRAS, 280, 1071

Mink, D. J. 1997, In: Hunt, G., Payne, H. E. (eds.) VI ASP Conf. Series, 125, Astronomical Data Analysis Software and Systems, 249

Monet, D., et al. 1996, USNO-SA1.0 Catalogue (Washington: US Nav. Obs.)

Novotny, E. 1973, In: Introduction to Stellar Atmospheres and Interiors, p. 226, Oxford University Press.

Nyman, L.-Å, Bronfman, L., & Thaddeus, P. 1989, A&A, 216, 185

Price, S. D., Egan, M. P., Carey, S. J., Mizuno, D. R., & Kuchar, T. A. 2001, AJ, 121, 2819

Reiputrh, B. 1981, A&AS, 44, 379

Rieke, G. H., & Lebofsky, M. J. 1985, ApJ, 288, 618

Schwartz, R. D. 1977, A&AS, 35, 161

Tapia, S. 1973, In: Greenberg, J. M., & van de Hulst, H. C. (eds.) IAU Symposium 52, Interstellar Dust and Related Topics, 43

Tomita, Y., Saito, T., & Ohtani, H., 1979, PASJ, 31, 407

Vaidya, D. B., Gupta, R., Dobbie, J. S., & Chylek, P. 2001, A&A, 584, 590

Vilas-Boas, J. W. S., Myres, P. C., & Fuller, G. A. 1994, ApJ, 433, 96

Weaver, W. B. 1974, ApJ, 189, 81

Zhou, S., Evans II, N. J., Kompe, C., & Walmsley, C. M., 1993, ApJ, 404, 232

Table 1. Off-Cloud Regions.

Region	α(2000.0)	δ(2000.0)
I	12 32 53	−64 21 34
II	12 32 55	−64 27 43
III	12 33 46	−64 26 34
IV	12 33 49	−64 22 44

Note. — Units of right ascension are hours, minutes, and seconds, and units of declination are degrees, arcminutes, and arcseconds.

Table 2. Candidate Pre-Main Sequence Stars with $K < 14.0$.

Star	α(2000.0)	δ(2000.0)	K	$H-K$	$J-H$
1	12 31 54.4	−63 50 00	13.99	0.66	0.90
2	12 32 05.0	−63 49 30	12.56	0.45	0.72

Note. — Units of right ascension are hours, minutes, and seconds, and units of declination are degrees, arcminutes, and arcseconds.

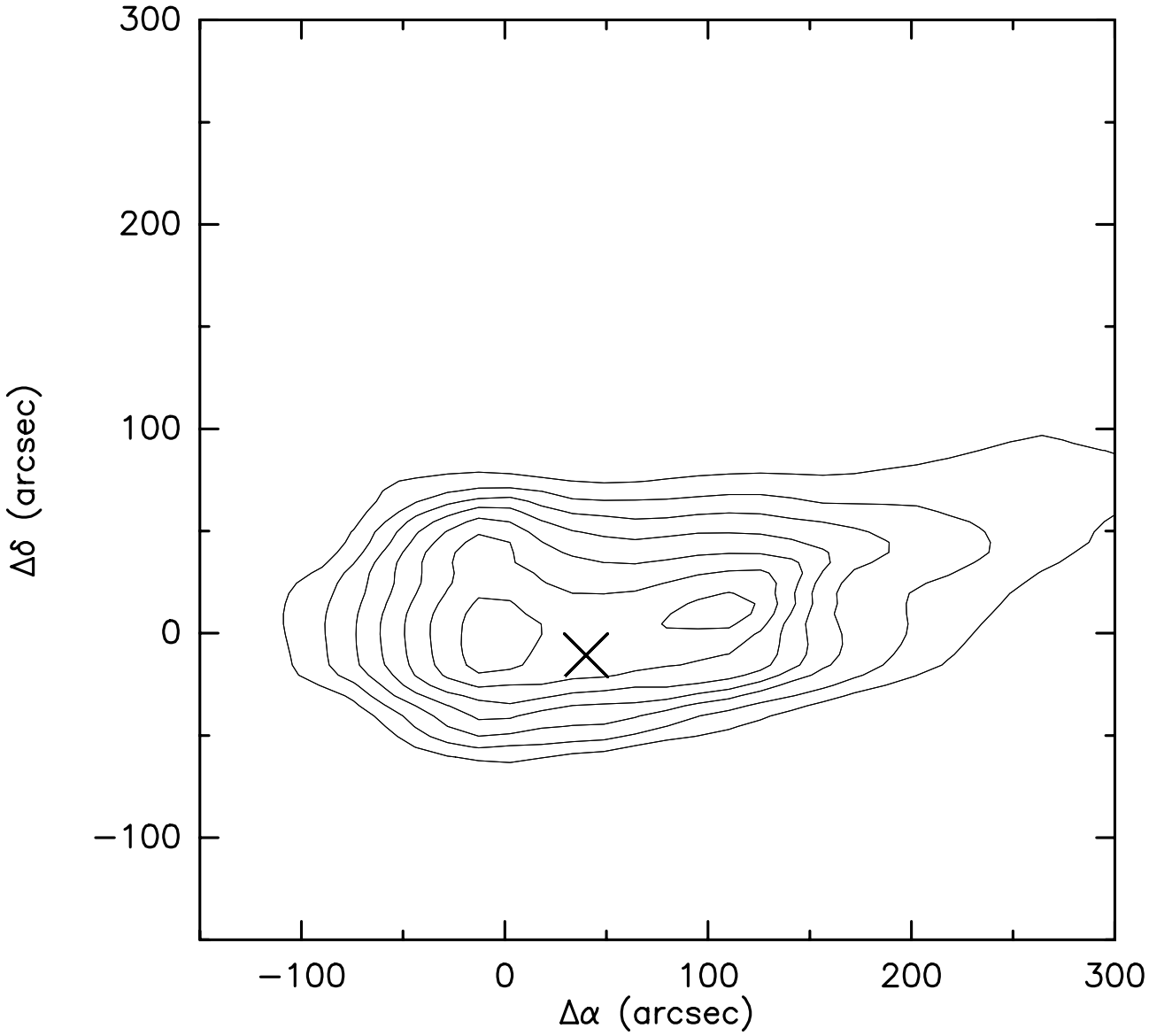
300
200
100
0
−100
Δδ (arcsec)
−100
0
100
200
300
Δα (arcsec)